Journal of Sol-Gel Science and Technology 33, 193–200, 2005

Template-Based Growth of Oxide Nanorod Arrays by Centrifugation

TIANLONG WEN*, JING ZHANG*, TAMMY P. CHOU, STEVEN J. LIMMER AND GUOZHONG CAO
Department of Materials Science and Engineering, University of Washington, 302 Roberts Hall, Box 352120, Seattle, WA 98195, USA
gzcao@u.washington.edu

Received April 12, 2004; Accepted June 30, 2004

Abstract. This paper reports template-based growth of nanorod arrays by combination of sol–gel processing and centrifugation. The technical concept is simple and straightforward; centrifugation force drives the sol nanoclusters into the pores of the template, filling the pores completely to form nanorods. However, simulation reveals the formation of nanorods inside pores is more complex; centrifugation force is insufficient to overcome the energy barrier that prevents agglomeration of two nanoclusters. Thermal fluctuation and solvent evaporation upon drying are considered to be the forces leading to the eventual agglomeration of concentrated nanoclusters inside template pores. Dense nanorods with ∼200 nm diameter and ∼10 μm length were readily obtained from polymeric SiO_2, colloidal SiO_2, TiO_2 and PZT sols after heat treatment.

Keywords: nanorod arrays, centrifugation, sol–gel processing, template-based growth

One of the most extensively studied and active areas of research have focused on the growth and formation of nanostructured oxide materials for their novel properties at the nanoscale and perspective applications in the field of nanotechnology. The driving force for nanotechnology has been miniaturization and exploration of new physical properties [1]. Many techniques have been utilized for the development and synthesis of nanostructured materials. A vapor-liquid-solid [2, 3] method by way of silicon nucleation and growth from the diffusion of gaseous Si into a drop of molten silicon-gold alloy has been employed to grow single crystal silicon nanorods in relatively large quantities. Laser-assisted catalytic growth [4, 5] has been done to produce *n*-type and *p*-type silicon nanowires. Electron beam lithography [6] and photolithography [7] have been widely used in the microelectronics industry to produce nanostructured materials. Template-assisted synthesis has shown to be effective methods for the formation of nanostructured materials, including metallic and polymeric nanorods [8–11], oxide nanorods [8, 9, 12, 13], and composite nanostructures [8, 14], and provide many advantages [15]—simple and inexpensive equipment, ease in processing, and low-temperature sintering. In this manner, the utilization of precursor solutions in conjunction with commercially available porous membranes allows for effective control of stoichiometry and structure morphology, and allows for straightforward compositional modification to produce nanostructures with complex stoichiometry.

Direct sol-filling and sol electrophoresis are two reported methods for the production of nanostructured materials by combining template synthesis and sol–gel processing. Martin et al. [8, 12] showed that TiO_2 nanorods could be formed by direct sol filling of template pores. They showed that the immersion of a template into a sol of oxide material allows for the penetration of sol particles into the pores. However, since capillary action is the only driving force for drawing the sol particles into the template pores, the packing density of these nanoclusters is small due to the relatively small capillary action and typically low solids content in sols. This could result in significant shrinkage, fracture or

*Present address: Sichuan University, Material Science & Engineering, Chengdu 610064, China.

deformation of the nanorods after heat treatment due to a large change in volume upon drying. Sol electrophoresis [15, 16] has been used to form dense, solid oxide nanorods to overcome potential problems from direct sol filling. In this method, an electric field is the driving force for pulling charged nanoclusters into the template pores to form dense nanostructures. These solid nanoclusters are stabilized and move in random motion in sol solutions due to an electrical double-layer along the surface. However, since the force acting on the nanoclusters by an electric field is determined by the magnitude of the zeta-potential of the nanoclusters, acidic or alkaline sols are required for effective nanostructure formation. A small absolute value of the zeta potential could also potentially result in poor structure formation due to a small force acting on the nanoclusters. Therefore, this method would be unfavorable for biologically active materials that are sensitive to acidic environments, and would be problematic for the incorporation of various functional groups or encapsulating elements in hybrid nanostructured materials that have negligible or limited surface charge.

In this paper, we report the formation of oxide nanorods by way of template-assisted centrifugation. The drawing of nanoclusters into the membrane pores is initiated by centrifugation force since the application of a force can aid these nanoclusters to move roughly in the direction of the applied force. The magnitude of the centrifugation force is determined by the mass of the nanoclusters and the rotation rate of the centrifuge. Thus, this method provides sufficient force for pulling nanoclusters into the template pores when a proper rotation rate is used. In addition, centrifugation is a versatile method that is not affected by the acidity of the sol, which is favorable for a wide variety of sol systems, including those consisting of biological species—proteins or enzymes—that may be sensitive to highly acidic or highly alkaline environments. Here, we show that template-assisted centrifugation is an effective method for the formation of nanorod arrays grown from polymeric silica (SiO_2), colloidal SiO_2, titania (TiO_2), and lead-zirconate-titanate ($Pb(Zr_{0.52}Ti_{0.48})O_3$, PZT) sols.

Experimental Section

Synthesis of Sols

Polymeric SiO_2 sol consisting of tetraethyl orthosilicate (TEOS 98%, Aldrich), ethanol (EtOH, 200 proof), deionized water (DI-H_2O), and hydrochloric acid (HCl 37.5%, Fisher Chemical) was initially used to explore the growth of oxide nanorods by centrifugation. The sol was prepared by dissolving TEOS in a solvent mixture of ethanol and DI water; HCl was then added to obtain a molar ratio of 1TEOS:1.5EtOH:1.8DI-H_2O:3.2×10^{-2}HCl, as previously reported [16]. The mixture was then stirred for approximately 2 h at room temperature. The SiO_2 sol, as prepared, resulted in negatively-charged SiO_2 particles with a pH value $\sim$3, which is above its isoelectric point (pH $\sim$ 2) [17]. Colloidal SiO_2 sol was commercially obtained (Nissan Chemical) consisting of 30–31wt% amorphous silica in 69–70 wt% isopropanol, and was used to further explore nanorod growth by centrifugation of SiO_2 particles with negligible surface charge. The TiO_2 sol was prepared from titanium (IV) isopropoxide (97%, Alfa Aesar), glacial acetic acid (Fisher Scientific), and DI water. The pH value of the sol is $\sim$2, below its isoelectric point (pH $\sim$ 6.2) [17], resulting in positively charged TiO_2 particles. The PZT sol was made from lead (II) acetate (99%, Alfa Aesar), glacial acetic acid (Fisher Scientific), titanium (IV) isopropoxide (97%, Alfa Aesar), zirconium (IV) *n*-propoxide (70% in propanol, Alfa Aesar), and DI water. The pH value of the sol is $\sim$4, also below its isoelectric point (pH $\sim$ 7.6) [17], resulting in positively charged PZT sol particles. Detailed information for the preparation of both TiO_2 and PZT sols was previously reported [16]. Table 1 gives a summary of the components for the preparation of the various oxide sols.

Synthesis of Nanorods

The formation of nanorods was done using a template-assisted centrifugation process. Track-etched hydrophilic polycarbonate (PC) membranes (Millipore, Bedford, MA) with 10 μm thickness and 200 nm diameter pores were used. Each PC membrane was securely placed flat at the bottom of a 13 mm diameter syringe tube and 3 mL of sol was added. The tube was sealed with Parafilm® and placed in a centrifuge tube. For the various oxide systems, centrifugation was performed at a rate of approximately 1400 revolutions per minute (RPM) for 60 min. Upon contact of the sol to the membrane, the sol was initially drawn into the membrane pores by capillary action, and the process of rotation initiated the migration of particles from the sol into the membrane pores by centrifugation force, resulting in the enrichment of solid within the pores. All the

Table 1. Summary of the preparation of the various oxide sol systems.

Material	Precursors	Solvents/other chemicals	Solids content (vol%)	pH
Polymeric SiO_2	Tetraethyl orthosilicate	Ethanol DI water Hydrochloric acid	~8.0	~3
Colloidal SiO_2	Silica	Isopropanol	~13	~2
TiO_2	Titanium (IV) isopropoxide	Glacial acetic acid DI water	~2.0	~2
PZT	Lead (II) acetate Titanium (IV) isopropoxide Zirconium (IV) n-propoxide	Glacial acetic acid DI water Lactic acid Glycerol Ethylene glycol	~5.0	~ 4

samples were rinsed with DI water after centrifugation and dried in air at approximately 100°C for 24 h. A drop of ITO sol was used to attach the samples to silica glass and allowed to dry in air at 100°C for another 24 h. The SiO_2, TiO_2 and PZT samples were then sintered at 600, 500, and 650°C, respectively, all for 60 min and with a ramping rate of approximately 2°C/min. High temperature sintering was done to burn off the PC membrane and to densify the nanorod structure. Scanning electron microscopy (SEM, JEOL 840A) was used to study the morphology of the nanorod structure of all the samples. Samples were sputter-coated with a thin Au/Pd layer prior to SEM observation. X-ray diffraction (XRD, Phillips PW1830) was also used to verify the phases and crystal structures of TiO_2 and PZT after sintering to high temperatures.

Results

Preliminary efforts indicate that template-assisted centrifugation results in the formation of nanorods of the desired oxide material. Figure 1 shows the SEM image of SiO_2 nanorods grown by centrifugation of polymeric SiO_2 sol with negatively charged SiO_2 particles at a rate of 1400 RPM for 60 min. This figure shows the top and side views of the SiO_2 nanorods attached to glass, respectively. From the figures, it can be seen that unidirectionally aligned, solid SiO_2 nanorods with good uniformity can be grown by centrifugation. The nanorods all have roughly the same diameter and length. The diameter is estimated to be approximately 170 nm, and is uniform throughout the entire length of the nanorod. Additionally, the length of the nanorods

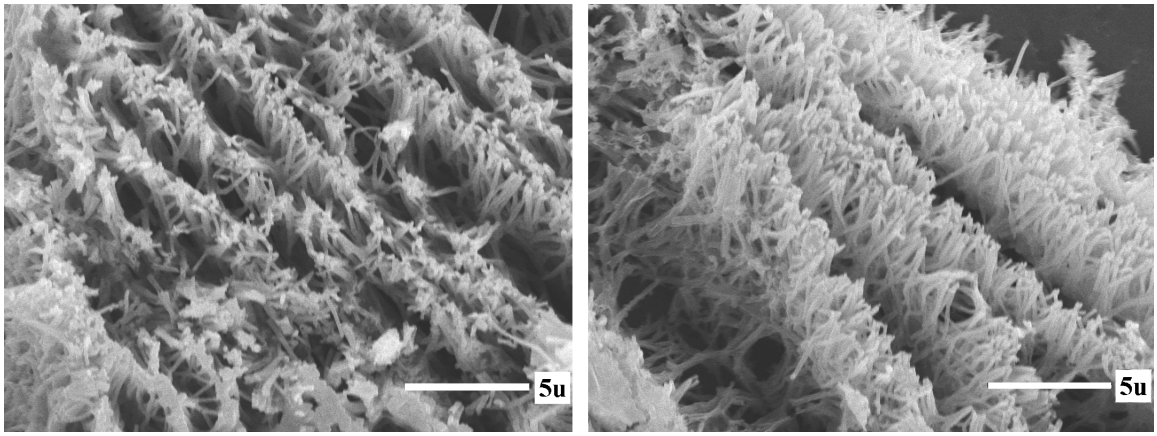

Figure 1. SEM images of the top view (left) and side view (right) of SiO_2 nanorods grown from polymeric SiO_2 sol by centrifugation at 1400 RPM for 60 min. Samples were attached to silica glass and sintered at 600°C for 60 min.

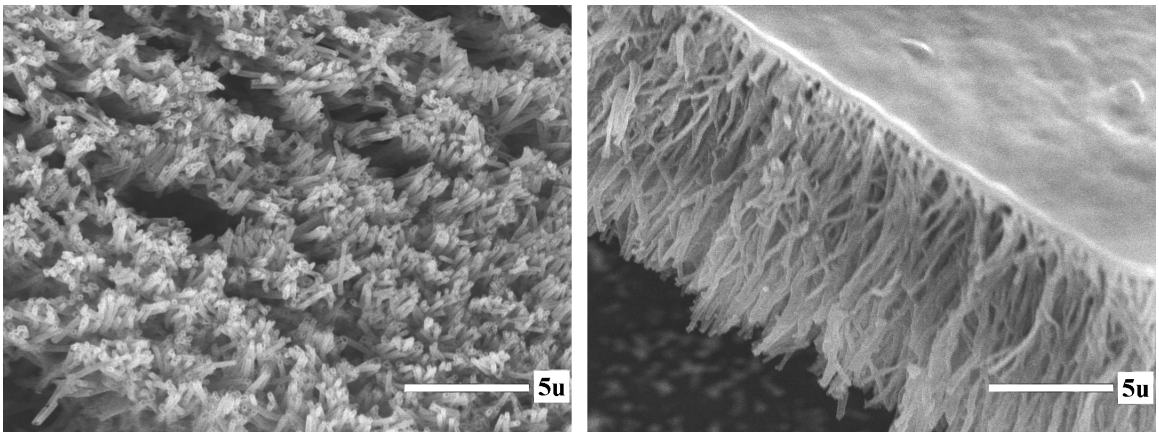

Figure 2. SEM images of the top view (left) and side view (right) of SiO_2 nanorods grown from colloidal SiO_2 sol by centrifugation at 1400 RPM for 60 min. Samples were attached to silica glass and sintered at 600°C for 60 min.

is also estimated to be approximately 10 μm, equivalent to the thickness of the template. Comparing the nanorod diameter with the membrane pore diameter, a lateral shrinkage is estimated to be ∼15%. The reduction in the nanorod diameter could be due to volume shrinkage caused by densification during the heat treatment process.

Figure 2 shows the SEM image of SiO_2 nanorods grown by centrifugation of colloidal SiO_2 sol with zero or negligible surface charge at a rate of 1400 RPM for 60 min. This figure displays the top and side views of the SiO_2 nanorods attached to glass, respectively. A thin layer can be seen on the top of the nanorod arrays. This is likely due to excessive deposition on the top of the membrane during centrifugation. The diameter of the nanorods is estimated to be approximately 200 nm, which is equivalent to the membrane pore diameter. The lack of appreciable reduction in the diameter of the nanorods indicates that significant densification of the nanorods may not have occurred during sintering, resulting in no lateral shrinkage. Although the majority of the nanorods are uniform, it can be seen that a number of nanorods are broken and nanotube formation also occurred. By comparison, the formation of uniform nanorods is possible by centrifugation regardless of the surface charge of the SiO_2 sol particles, but a few regions in Fig. 2 show the formation of nanotubes; whereas, the formation of nanotubes is not observed in Fig. 1. This inconclusively demonstrates that a difference in particle deposition may have an influence on the nanorod structure. Since the colloidal SiO_2 sol contains nanoclusters with a layer of organic groups on the surface, nanoclusters may have less close packing, forming a porous structure. Additionally, the presence of the organic groups may prevent densification during heat treatment since the burnout of the organic groups generates gaseous products and hinders the removal of pores. As a result, the lack of densification during heat treatment could have instigated the presence of broken and nonuniform nanorods, as well as the formation of hollow tubes.

Additional experimentation shows that centrifugation of TiO_2 and PZT sol systems can also be done to form solid nanorods. Figure 3 shows the top and side views, respectively, of TiO_2 nanorods formed from TiO_2 sol by centrifugation at 1400 RPM for 60 min and attached to glass. The TiO_2 nanorods were formed at a lower temperature relative to the other sol systems in order to preserve the anatase phase. Temperatures above 500°C would initiate phase transformation from anatase to rutile. Figure 4 shows the top and side views of PZT nanorods formed from PZT sol by centrifugation at 1400 RPM for 60 min and attached to glass, respectively. It can be seen in both cases that dense uniform nanorods unidirectionally-aligned were obtained. The nanorods have a uniform diameter throughout the entire length and have a relatively smooth surface. The estimated diameter of the TiO_2 and PZT nanorods is ∼150 and ∼130 nm, respectively. This indicates that significant lateral shrinkage occurred from sintering to high temperatures. A 25 and 35% reduction in diameter of the TiO_2 and PZT nanorods, respectively, shows that incomplete particle packing occurred during nanorod

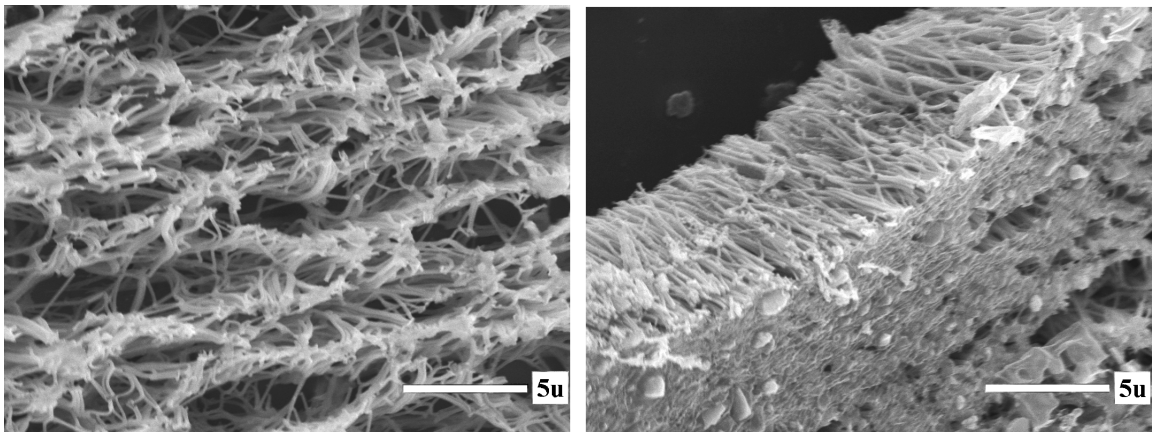

Figure 3. SEM images of the top view (left) and side view (right) of TiO_2 nanorods grown from TiO_2 sol by centrifugation at 1400 RPM for 60 min. Samples were attached to silica glass and sintered at 500°C for 60 min.

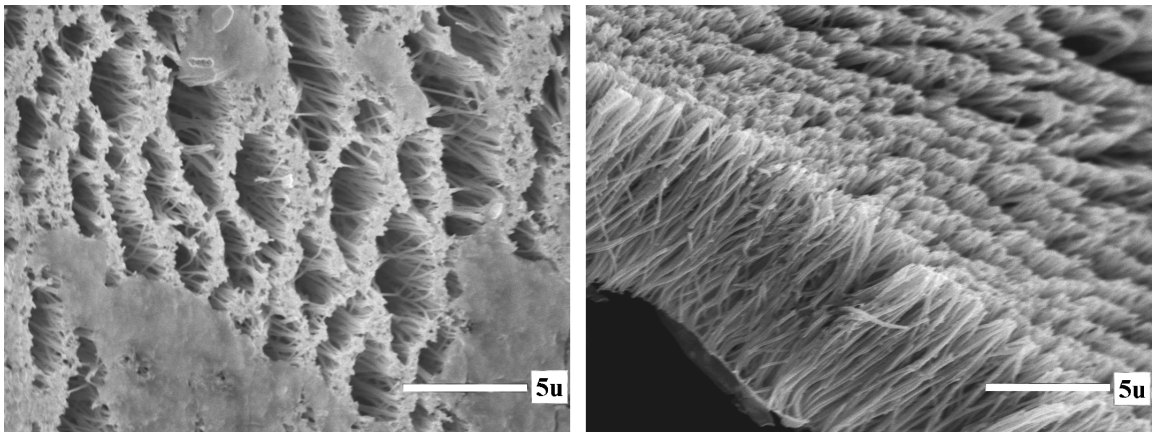

Figure 4. SEM images of the top view (left) and side view (right) of PZT nanorods grown from PZT sol by centrifugation at 1400 RPM for 60 min. Samples were attached to silica glass and sintered at 650°C for 60 min.

formation. By comparison, the nanoclusters in the TiO_2 and PZT sols did not pack as densely as the nanoclusters in the polymeric SiO_2 sol within the membrane pores. Table 2 gives an overview of the results of the four different types of nanorods grown by centrifugation. XRD spectra of TiO_2 and PZT nanorods are identical to the spectra of their respective powder samples. Neither preferential crystal orientation nor microstructure anisotropy was observed in centrifugation grown nanorods.

Table 2. Summary of the results of the four different types of nanorods.

Material	Sintering	Crystallinity	Diameter size (nm)	Shrinkage (%)
Polymeric SiO_2	600°C, 60 min	Amorphous	∼170	15
Colloidal SiO_2	600°C, 60 min	Amorphous	∼200	00
TiO_2	500°C, 60 min	Anatase	∼150	25
PZT	650°C, 60 min	Perovskite	∼130	35

Discussion

In order to understand the mechanism behind the formation of nanorods using centrifugation, we have to examine in more detail the movement of nanoclusters during the centrifugation process. Within the sol system, nanoclusters move randomly due to a combination of forces—Brownian motion and negligible gravity and buoyancy forces. During the centrifugation process, the centrifugation force is the predominant driving force for the movement of nanoclusters and a drag force exists in opposition. Analogous to the velocity of a particle undergoing sedimentation [17] (but replacing the acceleration due to gravity g with the centrifugal acceleration $\omega^2 R$), we have:

$$v = \frac{2a^2(\rho_s - \rho_l)\omega^2 R}{9\eta} \tag{1}$$

where a is the particle radius, ρ_s and ρ_l are the solid and liquid densities, ω is the rotation speed, R is the radius of the centrifuge and η is the sol viscosity. Substituting typical values for a sol ($a = 5 \times 10^{-9}$m, $\rho_s = 2 \times 10^3$ kg/m^3, $\rho_l = 1 \times 10^3$ kg/m^3, ω-145 rad/s, $R = 0.10$ m and η-1×10^{-3} (Pa^{-s}) [17] along with the values for the centrifuge used ($\omega = 145$ rad/s and $R = 0.10$ m) into Eq. (1), we can roughly estimate the velocity of the nanoclusters as ~1 nm/s. Since the length of the membrane pores are approximately 10 μm, it is found that the nanoclusters take ~15 min to move from the top of the pore membrane to the bottom of the pore membrane at a rate of ~1400 RPM, assuming no or negligible interaction between the nanoparticles and the template pore surface. Thus, 67 min are required to fill the template pores completely by nanoclusters. This estimation is based on 5 vol% solid nanoclusters in the sols, 30 vol% porosity in the PC membranes, and 74% packing density.

As the sol nanoparticles move down the template pores, they eventually approach the growth surface. While this surface is initially a second material (e.g., Al), after a short time the surface will be covered with the material being deposited. This surface is in contact with the sol, and will thus have a surface charge and establish a double layer structure, just like that of the sol nanoclusters. This will lead to an electrostatic repulsion between the incoming nanoparticles and the growth surface. Additionally, there will be attractive, van der Waals forces between the particles and the growth surface. The total energy of interaction (V_t) can be described as:

$$V_t = V_R + V_A \tag{2}$$

where V_R is the repulsive energy and V_A is the attractive energy. One can model the energies in this system as the interaction between a sphere and a flat plate, when no external forces are applied to the system. Using the Hogg-Healy-Fuerstenau (HHF) formula for the interaction, and assuming that the nanoparticle and the surface have the same zeta potential, V_R can be calculated as [18]:

$$V_R(H) = 2\pi\varepsilon_r\varepsilon_0 a\zeta^2\left\{\ln\left[\frac{1+\exp(-\kappa H)}{1-\exp(-\kappa H)}\right] + \ln[1-\exp(-2\kappa H)]\right\} \tag{3}$$

where H is the separation distance between the nanoparticle surface and the growth surface, ε_r is the dielectric constant of the liquid medium, ε_0 is the permittivity of a vacuum, a is the nanoparticle radius, ζ is the zeta potential, and κ is the Debye-Hückel parameter ($\kappa = (e^2 \sum n_i^0 z_i^2/\varepsilon_r\varepsilon_0 kT)^{1/2}$)[17]. Similarly, one can find the van der Waals interaction between a sphere and a plate as [19]:

$$V_A(h) = -\frac{A}{6}\left[\frac{1}{h} + \frac{1}{h+2} - \ln\left(\frac{h+2}{h}\right)\right] \tag{4}$$

where h is the dimensionless separation distance ($h = H/a$) and A is Hamaker's constant. Hamaker's constant for the nanoparticles/surface interacting through the liquid medium was calculated using the method described by Gregory [20]:

$$A = \frac{1}{\varepsilon_{r3}}\left(A_{11}^{1/2} - A_{33}^{1/2}\right)^2 \tag{5}$$

where A_{11} and A_{33} are the Hamaker constants for the sol material and the liquid interacting with themselves. Table 3 lists the Hamaker constants used in the energy calculations, along with the size of the calculated energy barrier. Where possible, reported values of the Hamaker constants were used (see References [21] and [22] for more information). For some of the data, however, exact values were unavailable, so that it was necessary to use approximate values. Additionally, the zeta potential values used to determine the repulsive energies are approximate values, determined by suspending the dry sol–gel powder in an aqueous solution at

Table 3. Hamaker constants and energies for selected sol systems.

Material	Zeta potential[a] (mV)	A_{11} ($\times 10^{-20}$J) [source]	A_{33} ($\times 10^{-20}$J) [source]	A (calculated) $\times 10^{-20}$J	Height of energy barrier ($\times 10^{-22}$ J)	Kinetic energy from centrifugation ($\times 10^{-45}$ J)
TiO_2	18.85	14.3 [21]	5 [22][b]	1.29	1.56	3.98
SiO_2	8.14	6.50 [21]	5 [22][b]	0.053	0.63	0.42
PZT	7.63	15 [22][c]	5 [22][b]	1.45	0.71	19.2

[a]Values are approximated and determined from suspending each sol–gel powder in aqueous electrolyte solution at pH similar to its respective sol system.
[b]This is an average value for organic solvents.
[c]This is an average value for oxides.

approximately the same pH and ionic strength. Such determined zeta potentials are also included in Table 3. These approximations yield values of the energy barrier which are not exact, but are still helpful for suggesting the general scale of energies involved.

Taking the velocity of the nanoparticles calculated earlier, one could determine the kinetic energy of each nanoparticle in the sol. For TiO_2, the value is about 3.98×10^{-45} J. This value can be compared to the height of the energy barrier calculated above, which is about 1.3×10^{-20} J for TiO_2. Obviously, the kinetic energy of the particles due to centrifugation is insufficient to bring the particles all the way to the growth surface, but they can approach quite closely. For example, TiO_2 and SiO_2 show secondary minima in their energy curves. Although the exact deposition mechanism is not known, there are two possibilities. One is that centrifugation enriches the nanoparticles in the close proximity of the growth surface, and thermal energy fluctuation allows the nanoparticles to overcome the energy barrier, make contact with and become bound to the growth surface, since the magnitude of the energy barrier is significantly smaller than kT. Another possibility is that centrifugation enriches and traps nanoparticles inside template pores only. Agglomeration of nanoclusters and formation of nanorods inside template pores occur only when the template was removed from the sol. When solvent evaporates during drying, the double layer structure collapses and nanoclusters agglomerate to form nanorods. Although both hypothetical mechanisms are possible, further experiments are needed to verify the deposition mechanisms.

Conclusions

In summary, we have shown that solid nanorods with dense, uniform structure can be synthesized by a combination of template-assisted centrifugation and sol–gel processing. Nanorods formed from electrostatically stabilized SiO_2, TiO_2 and PZT sols have shown to have a diameter of $\sim$170, $\sim$150, and $\sim$130 nm, respectively. The nanorods all have a length of $\sim$10 μm, equivalent to the thickness of the template. Further experiments and simulation suggest that the formation of nanorods inside template pores is likely attributable to the enrichment and entrapment of nanoparticles inside template pores by centrifugation and agglomeration of nanoclusters onto the growth surface by thermal energy fluctuation and/or solvent evaporation.

Acknowledgments

T. Wen and J. Zhang thanks the financial support by the UW Worldwide program under the direction of Prof. G. Kalonji. T.P. Chou thanks the Joint Institute of Nanoscience Fellowship, funded by the Pacific Northwest National Laboratory (operated by Battelle for the U.S. Department of Energy) and the University of Washington. S.J.L. would like to acknowledge financial support from the NSF-IGERT fellowship from the Center for Nanotechnology at the University of Washington.

References

1. G.Z. Cao, *Nanostructures and Nanomaterials: Synthesis, Properties and Applications* (Imperial College Press, London, 2004).
2. J. Westwater, D.P. Gosain, S. Tomiya, S. Usui, and H. Ruda, J. Vac. Sci. Tech. B **15**, 554 (1997).
3. Y. Xia, P. Yang, Y. Sun, B. Wu, B. Mayers, B. Gates, Y. Yin, F. Kim, and H. Yan, Adv. Mater. **15**, 353 (2003).
4. X. Duan and C.M. Lieber, Adv. Mater. **12**, 298 (2000).
5. Y. Cui, X. Duan, J. Hu, and C.M. Lieber, J. Phys. Chem. B **104**, 5213 (2000).

6. K. Kurihara, K. Iwadate, H. Namatsu, M. Nagase, and K. Murase, J. Vac. Sci. Tech. B **13**, 2170 (1995).
7. Y. Xia, J.A. Rogers, K.E. Pau, and G.M. Whitesides, Chem. Rev. **99**, 1823 (1999).
8. J.C. Hulteen and C.R. Martin, J. Mater. Chem. **7**, 1075 (1997).
9. A. Huczko, Appl. Phys. A **70**, 365 (2000).
10. L. Piraux, S. Dubois, and S. Demoustier-Champagne, Nucl. Instr. Meth. In Phys. Res. B **131**, 357 (1997).
11. C. Schonenberger, B.M.I. Van der Zande, L.G.J. Fokkink, M. Henry, C. Schmid, M. Kruger, A. Bachtold, R. Huber, H. Birk, and U. Staufer, J. Phys. Chem. B **101**, 5497 (1997).
12. B.B. Lakshmi, C.J. Patrissi, and C.R. Martin, Chem. Mater. **9**, 2544 (1997).
13. Y. Li, G.S. Cheng, and L.D. Zhang, J. Mater. Res. **15**, 2305 (2000).
14. V.M. Cepak, J.C. Hulteen, G. Che, K.B. Jirage, B.B. Lakshmi, E.R. Fisher, and C.R. Martin, J. Mater. Res. **13**, 3070 (1998).
15. S.J. Limmer, S. Seraji, M.J. Forbess, Y. Wu, T.P. Chou, C. Nguyen, and G.Z. Cao, Adv. Funct. Mater. **12**, 59 (2002).
16. S.J. Limmer and G.Z. Cao, Adv. Mater. **15**, 427 (2003).
17. R.J. Hunter, *Zeta Potential in Colloid Science* (Academic Press, London, 1981).
18. Y. Gu, J. Colloid Interf. Sci. **231**, 199 (2000).
19. Y. Gu and D. Li, J. Colloid Interf. Sci. **217**, 60 (1999).
20. J. Gregory, Advan. Colloid Interf. Sci. **2**, 396 (1969).
21. L. Bergström, Advan. Colloid Interf. Sci. **70**, 125 (1997).
22. J. Visser, Advan. Colloid Interf. Sci. **3**, 331 (1972).